PHILOSOPHICAL TRANSACTIONS A

rsta.royalsocietypublishing.org

Research

Cite this article: Boisse P, Hamila N, Madeo A. 2016 Modelling the development of defects during composite reinforcements and prepreg forming. *Phil. Trans. R. Soc. A* **374**: 20150269. http://dx.doi.org/10.1098/rsta.2015.0269

Accepted: 7 March 2016

One contribution of 22 to a Theo Murphy meeting issue 'Multiscale modelling of the structural integrity of composite materials'.

Subject Areas:
computational mechanics, mechanical engineering, materials science

Keywords:
composites, fabrics/textiles, finite-element analysis, wrinkling, second gradient, mesoscopic

Author for correspondence:
P. Boisse
e-mail: philippe.boisse@insa-lyon.fr

Modelling the development of defects during composite reinforcements and prepreg forming

P. Boisse[1], N. Hamila[1] and A. Madeo[2]

[1]LaMCoS, and [2]LGCIE, INSA-Lyon, Université de Lyon, 69621 Villeurbanne, France

PB, 0000-0001-5930-3047

Defects in composite materials are created during manufacture to a large extent. To avoid them as much as possible, it is important that process simulations model the onset and the development of these defects. It is then possible to determine the manufacturing conditions that lead to the absence or to the controlled presence of such defects. Three types of defects that may appear during textile composite reinforcement or prepreg forming are analysed and modelled in this paper. Wrinkling is one of the most common flaws that occur during textile composite reinforcement forming processes. The influence of the different rigidities of the textile reinforcement is studied. The concept of 'locking angle' is questioned. A second type of unusual behaviour of fibrous composite reinforcements that can be seen as a flaw during their forming process is the onset of peculiar 'transition zones' that are directly related to the bending stiffness of the fibres. The 'transition zones' are due to the bending stiffness of fibres. The standard continuum mechanics of Cauchy is not sufficient to model these defects. A second gradient approach is presented that allows one to account for such unusual behaviours and to master their onset and development during forming process simulations. Finally, the large slippages that may occur during a preform forming are discussed and simulated with meso finite-element models used for macroscopic forming.

This article is part of the themed issue 'Multiscale modelling of the structural integrity of composite materials'.

THE ROYAL SOCIETY PUBLISHING

1. Introduction

Composite materials with continuous fibres (carbon, glass, aramid, etc.) are used because of their good mechanical properties associated with low densities. Recent-generation military and civil aircraft make extensive use of composite materials for their primary structure. The use of lightweight materials is also an issue for the automotive industry which is faced by the new European regulation that requires a decrease in CO_2 emission to $95\,g\,CO_2\,km^{-1}$ in 2020 (3.7 litre/100 km) (http://ec.europa.eu/clima/policies/transport/vehicles/cars/documentation_en.htm). The development of lightweight vehicles is the only possibility for the automotive industry to comply with this future regulation. Among the various lightweight materials, composites appear as very promising materials and their development has attracted more and more attention in transportation [1,2].

The current manufacturing techniques of composite materials with continuous fibres take advantage of several processes. The increasing use of composite materials attracts attention to the idea of replacing the traditional (costly) experimental trial-and-error based methods with the optimization of processing parameters through numerical simulations and virtual manufacturing.

Liquid composite moulding (LCM) processes and prepreg draping (or forming) are two of the main families of composite manufacturing processes. In LCM processes, a (generally) thermoset resin is injected into a textile preform which is then cured at high temperature. Prepregs are semi-products made of continuous fibre reinforcements and thermoset or thermoplastic matrix. In the case of thermoset prepreg draping, the matrix is present but is not solid because it is not yet polymerized, thus the reinforcement can also be easily deformed. For continuous fibre thermoplastic prepreg forming, the matrix is heated above the melting temperature, and this permits deformation of the reinforcement, which can thus be shaped in its final form. Each of the processes mentioned above has its own specificity; however, shaping of the preforms for LCM processes, thermoplastic prepreg draping and thermoplastic prepreg thermoforming share the common feature of being obtained by the deformation of continuous fibre reinforcements. The matrix is absent for the preforming step of LCM processes. In thermosetting draping and thermoforming thermoplastic, the matrix plays an important role but the deformation of the prepregs is, nevertheless, controlled by those of the continuous fibre reinforcement. This deformation is specific. Movements are possible between the fibres, which allows high shearing deformation while the fibres are nearly inextensible in general.

Therefore, simulation software of these processes (LCM preform forming, thermoset prepreg draping and thermoplastic prepreg thermoforming) can have a common basis. Such a common basis can be used as a starting point for developing continuous fibre material forming software (with or without resin). On the other hand, constitutive laws, friction laws, specific finite elements and specific modules will be concerned in different processes. The reinforcements can be woven, unidirectional, non-crimp fabric (NCF), three-dimensional or interlocks. The simulation of the different forming processes for different composite materials requires a specific range of finite elements (shell, three-dimensional, solid shell) [3–7], of constitutive laws specific to these materials during forming [8–11] and friction laws [12–14].

Composite forming simulation codes have been developed with three main objectives [15–18]. Such codes aim to predict the composite state and geometry at the end of the forming, in particular, concerning the fibre directions, which will strongly influence the mechanical properties of the composite part. Secondly, the simulation can predict the conditions for a satisfactory manufacturing (loads on the tools, loads on a blank holder, speed, temperature, etc.). Thirdly, the simulation should predict the onset and the development of defects. There are several types of flaws that can be important depending on the process. Of course the three objectives mentioned above (prediction of the composite state and geometry, conditions for good manufacturing, prediction of defects) that are at the basis of an efficient composite reinforcement simulation are strongly connected. The main aim of this paper is to introduce possible modelling approaches of some defects. In a first instance, the simulation of wrinkling will be considered. The reason for

wrinkling onset, the growth and shape of the wrinkles will be analysed. Then, we will focus our attention on the onset of the shear transition zone: such zones in which bending of the fibres can be observed will be highlighted and modelled using a second gradient approach. The simulation of the loss of cohesion of a woven reinforcement during forming will be finally performed at the meso-scale during macroscopic forming analyses in order to allow slippage between the fibrous yarns.

2. Simulation of wrinkling of composite reinforcements during forming

(a) Explicit approach

Dynamic explicit approaches [19–21] are well suited to both forming and wrinkling simulations. The principle of virtual work associated with a finite-element approximation leads to:

$$\mathbf{M}\ddot{\mathbf{u}} + \mathbf{C}\dot{\mathbf{u}} = \mathbf{F}_{\text{ext}} - \mathbf{F}_{\text{int}}. \tag{2.1}$$

Here $\mathbf{M}$ and $\mathbf{C}$ are the mass and damping matrices, $\mathbf{F}_{\text{ext}}$ and $\mathbf{F}_{\text{int}}$ are the exterior and interior nodal loads, and $\mathbf{u}$ is the nodal displacement vector. In explicit codes, this equation is solved at each time step $\Delta t^i = t^{i+1} - t^i$ using the central difference scheme:

$$\mathbf{u}^{i+1} = \mathbf{u}^i + (\dot{\mathbf{u}}^{i-1/2} + \tfrac{1}{2}(\Delta t^{i-1} + \Delta t^i)\mathbf{M}_{\text{D}}^{-1}(\mathbf{F}_{\text{ext}}^i - \mathbf{F}_{\text{int}}^i - \mathbf{C}\dot{\mathbf{u}}^{i-1/2}))\Delta t^i. \tag{2.2}$$

The mass matrix is made diagonal in $\mathbf{M}_{\text{D}}$ [22]. The stability of the scheme needs to use sufficiently small time increments [23]. In composite reinforcement forming or prepreg thermoforming, shell finite elements are usually used. The specific mechanical behaviour is included in the interior nodal loads $\mathbf{F}_{\text{int}}^i$. A simulation based on equations (2.1) and (2.2) taking into account the shell kinematics and the specific mechanical behaviour describes the onset and development of eventual wrinkles during forming. A simplified shell finite element made of woven unit cells is briefly presented below. It is used to analyse the reason for wrinkling developments.

(b) Shell finite element made of textile reinforcement

A triangular finite element made of woven cells is shown in figure 1*a*. Neighbouring elements are used to calculate the curvatures in the elements and consequently to take bending into account [24]. The element is composed of *n*cell textile woven unit cells. The internal virtual work associated with a virtual displacement field $\boldsymbol{\eta}$ is assumed to be the sum of the virtual works of tension, in-plane shear and bending:

$$W_{\text{int}}(\boldsymbol{\eta}) = W_{\text{int}}^{\text{t}}(\boldsymbol{\eta}) + W_{\text{int}}^{\text{s}}(\boldsymbol{\eta}) + W_{\text{int}}^{\text{b}}(\boldsymbol{\eta}), \tag{2.3}$$

where

$$W_{\text{int}}^{\text{t}}(\boldsymbol{\eta}) = \sum_{p=1}^{n\text{cell}} {}^p\varepsilon_{11}(\boldsymbol{\eta})\,{}^pT_1\,{}^pL_1 + {}^p\varepsilon_{22}(\boldsymbol{\eta})\,{}^pT_2\,{}^pL_2 \quad \text{(virtual work of tension)}, \tag{2.4}$$

$$W_{\text{int}}^{\text{s}}(\boldsymbol{\eta}) = \sum_{p=1}^{n\text{cell}} {}^p\gamma(\boldsymbol{\eta})\,{}^pM^{\text{s}} \quad \text{(virtual work of in-plane shear)} \tag{2.5}$$

and

$$W_{\text{int}}^{\text{b}}(\boldsymbol{\eta}) = \sum_{p=1}^{n\text{cell}} {}^p\chi_{11}(\boldsymbol{\eta})\,{}^pM^{11}\,{}^pL_1 + {}^p\chi_{22}(\boldsymbol{\eta})\,{}^pM^{22}\,{}^pL_2 \quad \text{(virtual work of bending)}. \tag{2.6}$$

Here ${}^p\varepsilon_{11}(\boldsymbol{\eta})$, ${}^p\varepsilon_{22}(\boldsymbol{\eta})$, ${}^p\gamma(\boldsymbol{\eta})$, ${}^p\chi_{11}(\boldsymbol{\eta})$ and ${}^p\chi_{22}(\boldsymbol{\eta})$ are the virtual warp and weft axial strains, in-plane shear angle, and warp and weft curvatures in the cell p, respectively; L_1 and L_2 are the length of the woven cell in warp and weft directions; T^{11} and T^{22} are the tensions on the unit woven cell in

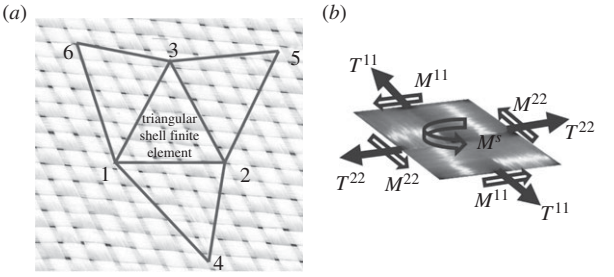

Figure 1. (*a*) Triangular shell finite element 1, 2, 3 made of woven cells and its neighbours and (*b*) load resultants on a woven cell.

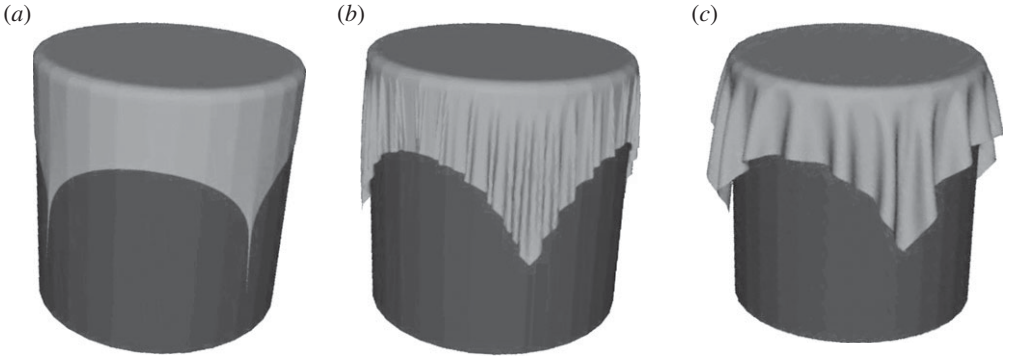

Figure 2. (*a*) Draping simulation with tensile stiffness only, (*b*) with tensile and in-plane shear stiffnesses and (*c*) with tensile, in-plane shear and bending stiffnesses.

warp and weft directions; M^{11} and M^{22} are the bending moments on the woven cell, respectively, in warp and weft directions; and M^s is the in-plane shear moment (figure 1*b*).

The shell finite element made of textile woven cells (figure 1*a*) is used to analyse wrinkle onset and development. As shown in figure 1*b* each woven cell is submitted to tension, in-plane shear and bending following equations (2.3)–(2.6). The interior nodal loads of tension, in-plane shear and bending can be obtained from those load resultants and the corresponding interpolation matrices of the element [25,26]. For bending, the curvatures are computed using the neighbouring elements.

(c) Simulation of wrinkle development in textile reinforcement forming

In sheet forming, wrinkling is a major issue because of the thinness of the sheet [27,28]. The bending stiffness of textile reinforcements is weak because of possible slip between fibres. Consequently, the wrinkling phenomenon is specific and frequent for these textile materials. Experimental analyses of wrinkling have been realized mainly in in-plane shear [29–34]. These studies generally use the 'shear locking angle' as a condition for wrinkle onset. This will be criticized in the sequel. Simulation of wrinkling has been proposed which is based on truss elements [4], membrane elements [35] or, recently, on beam and shell elements [36–38].

In this section, simulations based on the shell finite element briefly presented above are performed to highlight the parameters influencing wrinkle developments. The draping of an initially square woven textile reinforcement on a revolution cylinder is considered in figure 2. In figure 2*a*, only the tensile stiffness is considered (equation (2.4)). In-plane shear and bending are neglected. Draping does not lead to any wrinkles, but the shear angles are close to 90° in the corners of the fabric blank.

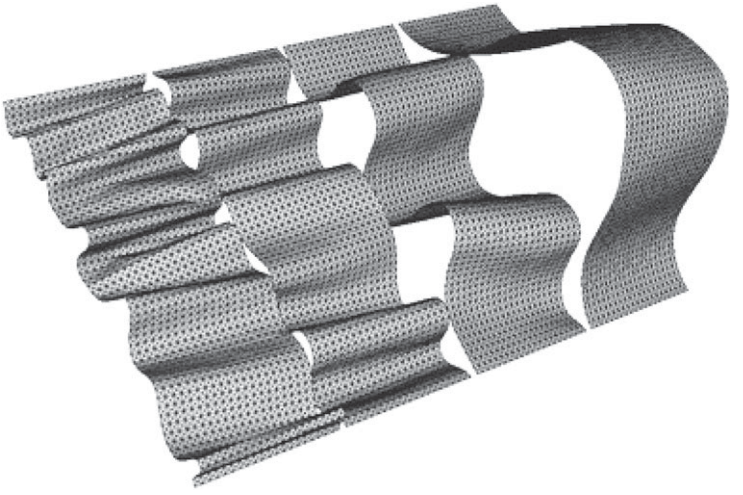

Figure 3. Wrinkling in compression of a woven reinforcement strip with different bending stiffness (from left to right 1, 10, 10^2, 10^3 N mm^{-1}).

The addition of in-plane shear stiffness (equation (2.5)) in the simulation leads to wrinkling. The wrinkles are small and numerous (figure 2*b*). Finally, the addition of bending stiffness, i.e. the complete use of equations (2.3)–(2.6), leads to larger and more realistic wrinkles (figure 2*c*). Globally, this example shows that the tensile stiffness leads the forming from quasi-inextensibility of the fibres. In-plane shear stiffness leads to wrinkling when the shear angles are large. Nevertheless, the onset of wrinkles depends also on other terms in equations (2.1) and (2.3). This will be discussed later. Finally, bending stiffness is important for wrinkle shape. This is detailed in the test presented in figure 3.

A $80 \times 20\,\text{mm}^2$ fabric strip is submitted to a compression in the yarn direction (40 mm). The size of the wrinkles increases (and their number decreases) with bending stiffness. In such a compression situation, wrinkle onset is quasi-immediate. Nevertheless, forming processes are generally designed to avoid these states of compression in the yarn direction. On the other hand, in-plane shear cannot be avoided because it is the requested deformation mode to obtain double curved shapes. That is why in-plane shear appears as the principal reason for wrinkle onset.

Figure 4 shows the forming of a textile reinforcement using a tetrahedral punch (figure 4*a*,*b*). This forming process has been studied in the context of the ITOOL European project [39,40]. There is no wrinkle in the tetrahedral part of the preform, thanks to blank holders that create tension in the yarns. On the other hand, many wrinkles develop in the horizontal part of the preform. The simulation using the shell element presented in §2.1 is shown in figure 4*d*. It is in good agreement with experimental forming. In particular, wrinkles are correctly simulated [40].

In zone A (figure 4*b*,*c*), the in-plane shear after forming is very large and reaches 60°. This value is also obtained by the simulation (figure 4*d*). Yet no wrinkles have developed in this zone (figure 4*c*). This is due to the blank holders that create strong tensions and avoid wrinkling. This case clearly shows the limit of the 'locking angle' concept. According to this notion, woven reinforcement wrinkling starts when this locking angle is reached. That is not the case in zone A where shear angles reach 60° and no wrinkles have developed. On the other hand, in the horizontal part of the preform there are wrinkles in zones where the in-plane shear angle is less than 40°. In figure 3, many wrinkles have developed and the shear angle is close to zero. Actually, wrinkle onset and development depend on all the (tension, in-plane shear and bending strain) energies (equations (2.1)–(2.6)). Wrinkles develop when the minimization of potential energy (i.e. the solution of dynamic equation (2.1)) leads to out-of-plane solutions. To determine if wrinkles will develop, all the strain energy (tension, in-plane shear and bending) must be taken into account.

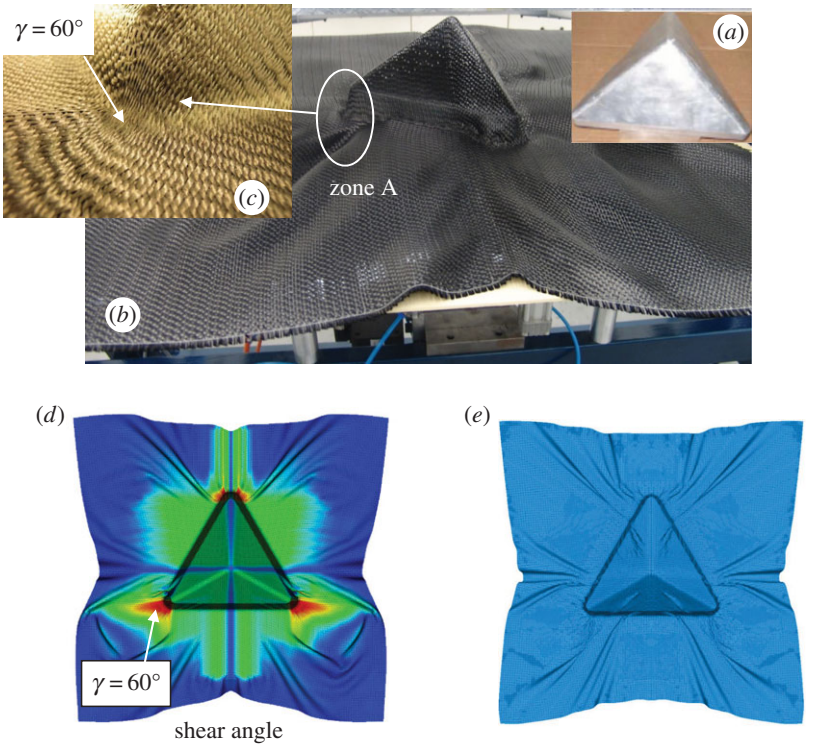

Figure 4. Forming of a tetrahedral shape: (*a*) tetrahedral punch, (*b*) shaped preform, (*c*) 60° shear angle in a corner, (*d*) forming simulation and (*e*) forming simulation with a low blank holder load.

Figure 4*e* shows the result of the simulation when the blank holder load is decreased from 1 bar to 0.2 bar. In this case, wrinkles propagate to the tetrahedral part which is the useful part of the preform. This has been confirmed experimentally [40].

3. Transition zones and second gradient approach

(a) Transition zone in preforms

Recent papers have highlighted another type of defect that can develop when the geometry of the preform leads to adjacent areas with constant but different shear angle. 'Transition zones' are observed between these areas. For instance, curvatures of the yarns are observed on a face of the tetrahedral shape analysed in §2 (figure 5*a*) and on the face of a prismatic preform (figure 5*c*) [41,42]. These yarn curvatures can lead to buckles (figure 5*b*). Similar transition zones have also been highlighted in bias extension tests [43]. The standard analysis of the test is based on two assumptions: inextensibility of the fibres and rotations at the yarn crossovers without slippage. The deformed shape of a specimen subjected to a bias extension test shows the development of areas with constant fibre orientations (zones A, B, C in figure 5*e*). Figure 5*d* shows transition zones between the areas A, B and C [43,44]. These transition zones (figure 5) are related to the bending stiffness of fibres. Such local bending is a property of the microstructure of the textile reinforcement. Some macroscopic properties of a textile material are low because of the possible slippage between the fibres. Nevertheless, the local (or micro) bending stiffness of the fibres plays a role, in particular, in the transition zones described above in which bending of the yarns can be observed. It is not possible to take account of these local properties in a standard continuum mechanics of Cauchy (or first gradient) approach. Actually, the properties of this macroscopic model are fixed by the possible slippage between the fibres that will lead (generally) to low global rigidities.

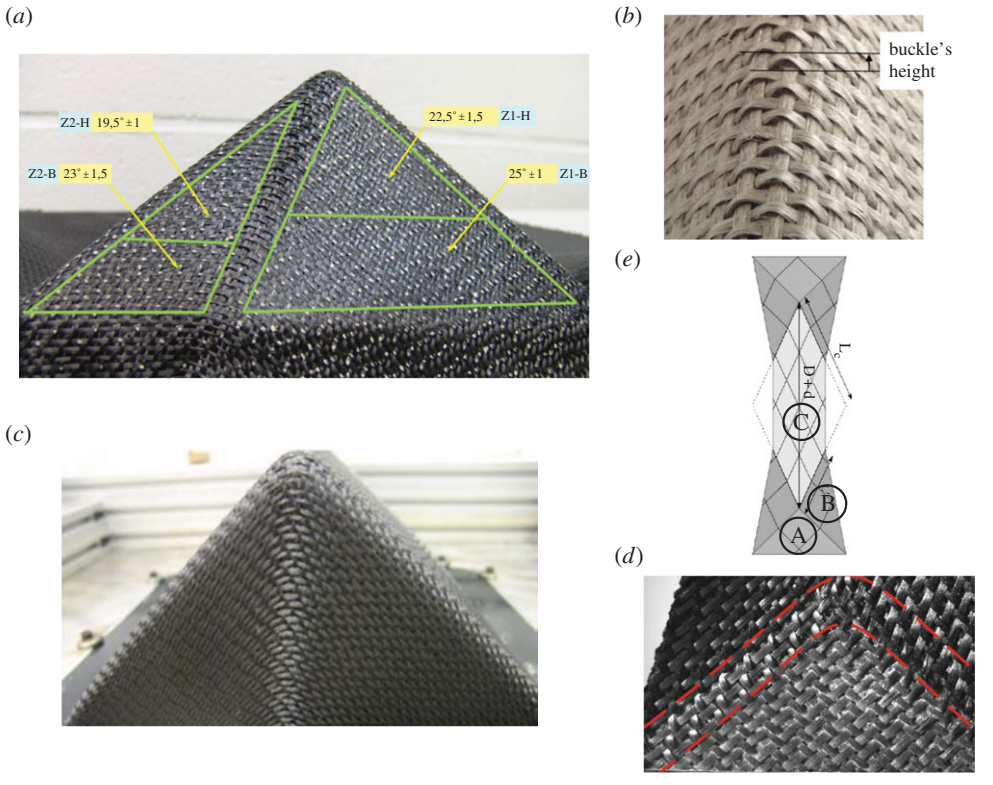

Figure 5. Defects in preform manufacturing: (*a*) transition zones on the face of a tetrahedron shape, (*b*) buckles on one edge of a tetrahedron shape, (*c*) transition zones on the face of prismatic shape and (*d*) transition zones in (*e*) a bias extension test.

(b) Second gradient approach

In order to account for fibre bending stiffness, a second gradient approach is a possible solution [43–45].

Denoting by $\mathbf{F}$ the deformation gradient and by $\mathbf{C} = \mathbf{F}^{\mathrm{T}} \cdot \mathbf{F}$ the right Cauchy–Green deformation tensor, the following orthotropic invariants are introduced for an in-plane two-dimensional problem as:

$$I_4 = \mathbf{M}_1 \cdot \mathbf{C} \cdot \mathbf{M}_1, \quad I_6 = \mathbf{M}_2 \cdot \mathbf{C} \cdot \mathbf{M}_2 \quad \text{and} \quad I_8 = \mathbf{M}_1 \cdot \mathbf{C} \cdot \mathbf{M}_2. \tag{3.1}$$

Here $\mathbf{M}_1$ and $\mathbf{M}_2$ are orthonormal vectors in the warp and weft directions in the initial configuration. The invariants I_4 and I_6 measure the changes of length in warp and weft; and I_8 is related to the angle variation between warp and weft yarns. A possible strain energy density is of the form:

$$\mathrm{W} = \frac{K_4}{2}(I_4 - 1)^2 + \frac{K_6}{2}(I_6 - 1)^2 + \frac{K_8}{2}(I_8)^2 + \frac{A_8}{2}(I_8)^p + \frac{\alpha}{2}\nabla I_8 \cdot \nabla I_8. \tag{3.2}$$

This strain energy density includes a second gradient term that takes into account the gradients of shear angle; α is the associated material parameter; and K_4 and K_6 are the warp and weft tensile rigidities. The tensile behaviours are assumed to be linear for simplicity purpose; K_8 and A_8 account for linear and nonlinear in-plane shear strains, respectively.

(c) Simulation of transition zones

The bias extension test is simulated both with a standard approach (first gradient) and with a simulation based on the strain energy density presented in equation (3.2) [43–45].

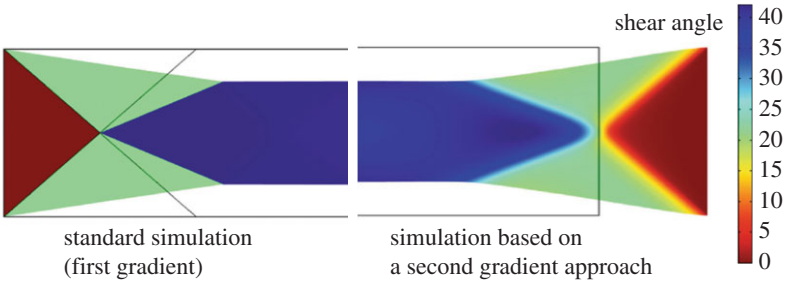

Figure 6. Simulation of the bias extension test using a standard approach and simulation based on a second gradient approach.

The finite-element mesh has been chosen in order to avoid locking that can occur in this case [46,47]. The simulation based on a first gradient approach gives the solution close to the 'fishnet' theory of the test. There are three zones with strictly constant in-plane shear in each zone. This is globally correct, but the transition zones shown in figure 5*d* are not described. The simulation based on the strain energy density with a second gradient term in in-plane shear gives in-plane shear patterns that are close to the real solution in the specimen. But, in addition, it correctly describes the transition zone corresponding to the fibre bending between two areas with constant in-plane shear (figure 6). This approach has been used to give solutions to other cases in which the fibre bending stiffness is important and where the standard simulations fail to give correct results [45]. The use of second gradient models for the simulation of forming cases where transition zones develop as in figure 5*a*,*c* is in progress.

4. Mesoscopic analyses: slippage between yarns

(a) Slippage during reinforcement forming

Large slippage between yarns can appear during a reinforcement forming process. Figure 7*a* shows such slippage in the vertical face of a prismatic preform made of glass plain weave fabric [41]. In figure 7*b*, a thermoplastic prepreg has been manufactured by thermoforming. The temperature was too low at the edge of the part which prevents correct forming deformation. Internal slip leads to a zone with only warp yarns (and no weft yarns). Figure 7*c* presents a hemispherical forming test for which the blank holder was intentionally tightened in order to create such slippage between the warp and weft yarns. The objective of this forming experiment was the validation of the forming simulation in the case of such slippages.

(b) Mesoscopic finite-element analyses

The slippage highlighted above leads to a loss of continuity of the textile reinforcement. The simulation of their development can hardly be considered at the macroscopic scale. Many composite analyses are performed at the mesoscopic scale, i.e. the scale of the fibrous yarns. For periodic structures, homogenized properties of the composite can be computed by mesoscopic analyses [48,49] and damage initiation and crack propagation [49–53]. The simulation of the resin flow within deformed woven cells allows one to compute the permeability of the reinforcement for different deformations [54]. These meso finite-element models are usually performed on one or a few representative unit cells (RUCs) with a fine mesh. The quality of these mesoscopic meshes of the RUCs strongly influences the quality of meso analyses [55–57].

To simulate the slippage onsets and developments such as those highlighted above, it is necessary to perform a meso finite-element simulation of the forming process, i.e. of all the woven cells in the preform, which means hundreds or thousands of RUCs. Consequently, it

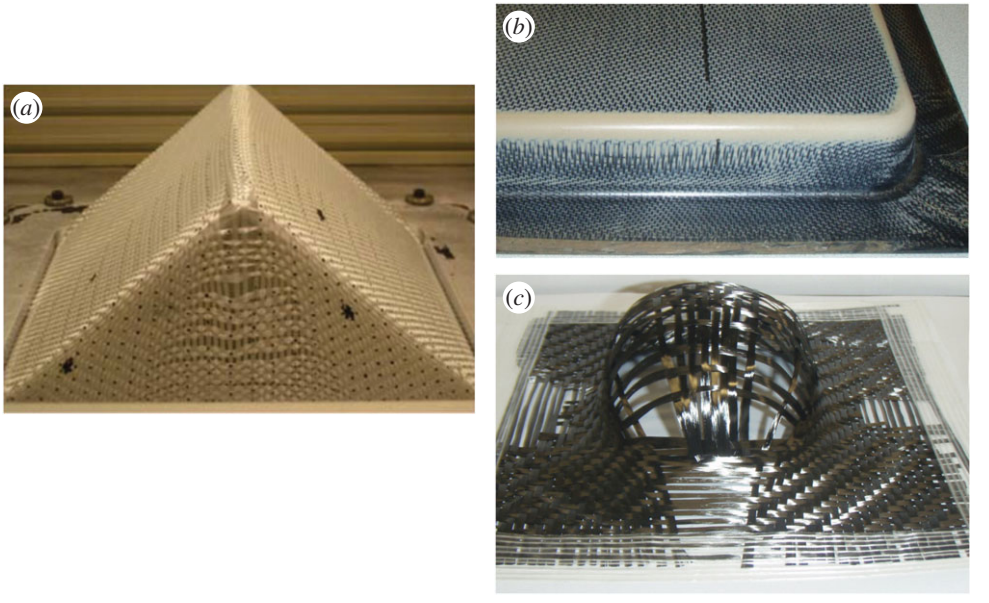

Figure 7. Slippage between yarns of textile reinforcements: (*a*) glass plain weave prismatic preform, (*b*) thermoplastic prepreg and (*c*) carbon twill fabric. (Online version in colour.)

is not possible to use meshes as fine as in analyses carried out on one or a few unit cells. In fact, to be able to simulate the forming of the whole part, the finite-element model of a woven cell has to be simple enough while describing the main phenomena at the mesoscopic scale. Different approaches are developed for the purpose of the simulation of the deformation of a whole preform with meso finite-element models [58–60].

In this work, each woven unit cell is modelled as a set of shell elements as shown in figure 8*a*. This model is very simplified. There are 416 d.f. per unit cell, which enables one to perform the whole preform forming simulations. Regardless of this simplicity, the main features of the woven cell behaviour are described. In particular, the contact with friction between the yarns allows rotation at the crossover of yarns. When the shear angle becomes large, the lateral contact between yarns increases the in-plane shear stiffness.

The mechanical behaviour of each yarn is those of a fibrous tow. It is described by a hypoelastic model with an objective derivative based on the fibre rotation [56,61]. An important feature is the possible slippage between the yarns which is allowed by the proposed mesoscopic model. The theoretical analysis of the bias extension test is based on the assumption that there is no slip at the yarn crossover. This assumption is correct for shear angles smaller than 35° or 40°. Then slippage occurs and the shear angle (measured by optical method) is smaller than the theoretical one (figure 8*c*). It is shown in figure 8*b*,*c* that the meso finite-element analysis of the bias extension test gives results consistent with the experiments even for large angles when the test theory is no longer verified. This agreement is possible because of the possible slippage between the yarns in the meso finite-element model. Figure 8*d*,*e* shows the results of meso finite-element analyses of the hemispherical shaping and prismatic shaping simulations. The corresponding experimental forming are shown in figure 7*a*,*c*, respectively [62,63]. In both cases, the forming process leads to strong defects due to large slippage between the yarns. These slippages are correctly described by the meso finite-element simulations. They are in correct agreement for the hemispherical forming (figures 7*c* and 8*d*), but the slippages are more important in the simulation of the prismatic forming (figures 7*a* and 8*e*). Actually, in the case of the hemispherical forming, the material parameters of the carbon twill have been measured in the laboratory, in particular, the friction between the yarns. This is not the case for the prismatic forming. Furthermore, the

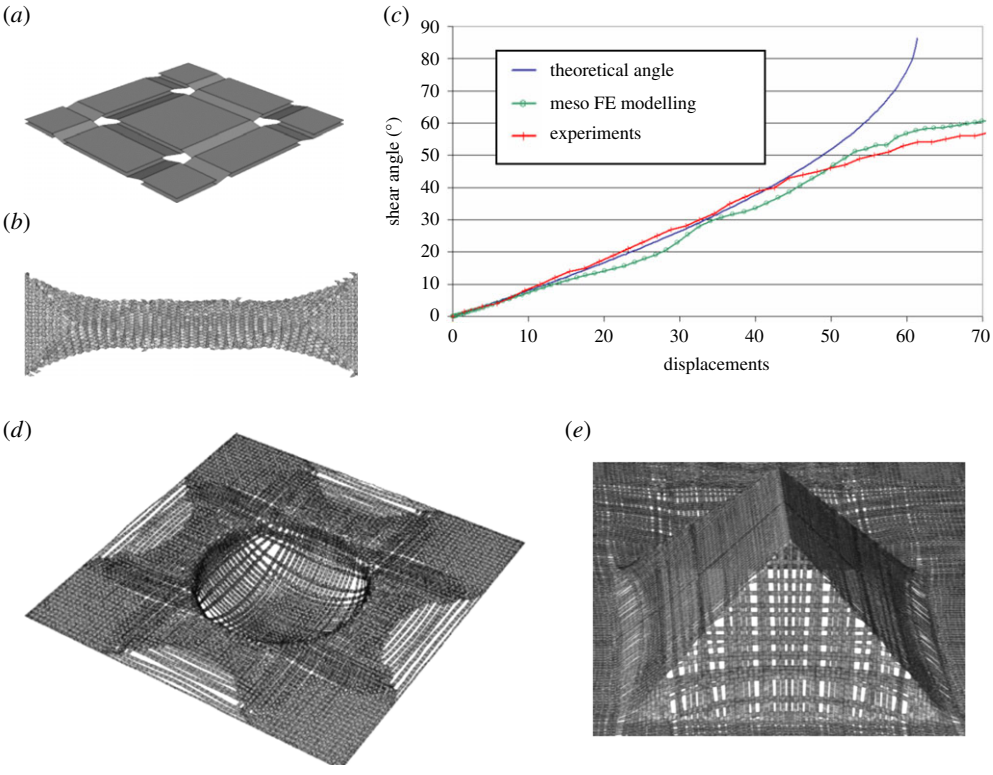

Figure 8. (*a*) Simplified finite-element model of the woven unit cell, (*b*) meso analysis of the bias extension test, (*c*) comparison of the shear angles, (*d*) meso finite-element simulation of a hemispherical forming with slippages and (*e*) meso finite-element simulation of a prismatic forming.

boundary conditions and more precisely the loads at the edge of the preform are very important for slippage. They are difficult to assess in many cases.

Nevertheless, the two presented meso finite-element simulations of preform stamping processes have shown that this approach is a possible way for the simulation of possible slippages during textile composite reinforcement forming.

5. Conclusion

Predicting defect onset and development is one of the main tasks of composite process simulations. Some defects are specific to textile composite reinforcement draping because of the internal structure that is made of fibres. The possible slip between fibres makes wrinkling frequent. Wrinkling is indeed one of the most common flaws during textile reinforcement forming. An explicit dynamic approach associated with a simplified behaviour of shell elements made of woven cells proved itself to be well suited to wrinkle modelling. It has been shown that the three parts of the strain energy (tension, in-plane shear and bending) have a role in wrinkling. If large shear angles that are necessary for double curved preforms can sometimes lead to wrinkling, there is no direct relation between shear angle and wrinkling. In particular, large tensions due to the blank holder can avoid wrinkling although shear angles are very large. Consequently, the 'locking angle' is a questionable concept for the determination of the wrinkling onset and must be used cautiously. The size of wrinkles depends on bending stiffness. Membrane approaches are frequent in draping simulations but they cannot describe wrinkle shapes.

'Transition zones' have been highlighted in several preform forming processes and in the bias extension test. First and second gradient approaches were compared in the simulation of the bias

extension test. Only the second gradient is able to describe the 'transition zones'. This approach is now introduced in forming simulation in order to simulate forming with 'transition zones' such as those shown in this paper.

Macroscopic forming (i.e. forming of the whole preform) based on mesoscopic models of the reinforcement is probably a promising way to go in composite preform draping simulations. It was shown that this meso finite-element modelling can simulate large slippage between the yarns during forming. More efficient numerical methods will be necessary for the expansion of this approach and to be able to develop meso finite-element models as efficient as macroscopic simulations.

Authors' contributions. P.B. designed the study, coordinated the study and drafted the manuscript; N.H. carried out the numerical methods; A.M. carried out the second gradient approaches; all authors gave final approval for publication.

Competing interests. The authors declare that they have no competing interests.

Funding. This research was supported by the National Scientific Research Centre (CNRS) in the scope of the project PEPS INSIS, and by the European Commission in the scope of the project ITOOL.

References

1. Fuchs ER, Field FR, Roth R, Kirchain RE. 2008 Strategic materials selection in the automobile body: economic opportunities for polymer composite design. *Compos. Sci. Technol.* **68**, 1989–2002. (doi:10.1016/j.compscitech.2008.01.015)
2. Friedrich K, Almajid AA. 2013 Manufacturing aspects of advanced polymer composites for automotive applications. *Appl. Compos. Mater.* **20**, 107–128. (doi:10.1007/s10443-012-9258-7)
3. Sharma SB, Sutcliffe MPF. 2004 A simplified finite element model for draping of woven material. *Composites A* **35**, 637–643. (doi:10.1016/j.compositesa.2004.02.013)
4. Skordos AA, Monroy Aceves C, Sutcliffe MP. 2007 A simplified rate dependent model of forming and wrinkling of pre-impregnated woven composites. *Composites A* **38**, 1318–1330. (doi:10.1016/j.compositesa.2006.11.005)
5. Ten Thije RHW, Akkerman R, Huétink J. 2007 Large deformation simulation of anisotropic material using an updated Lagrangian finite element method. *Comput. Methods Appl. Mech. Eng.* **196**, 3141–3150. (doi:10.1016/j.cma.2007.02.010)
6. Bel S, Hamila N, Boisse P, Dumont F. 2012 Finite element model for NCF composite reinforcement preforming: importance of inter-ply sliding. *Composites A* **43**, 2269–2277. (doi:10.1016/j.compositesa.2012.08.005)
7. Mathieu S, Hamila N, Bouillon F, Boisse P. 2015 Enhanced modeling of 3D composite preform deformations taking into account local fiber bending stiffness. *Compos. Sci. Technol.* **117**, 322–333. (doi:10.1016/j.compscitech.2015.07.005)
8. Peng XQ, Cao J. 2005 A continuum mechanics-based non-orthogonal constitutive model for woven composite fabrics. *Composites A* **36**, 859–874. (doi:10.1016/j.compositesa.2004.08.008)
9. Yu WR, Harrison P, Long A. 2005 Finite element forming simulation for non-crimp fabrics using a non-orthogonal constitutive equation. *Composites A* **36**, 1079–1093. (doi:10.1016/j.compositesa.2005.01.007)
10. Aimène Y, Vidal-Sallé E, Hagège B, Sidoroff F, Boisse P. 2010 A hyperelastic approach for composite reinforcement large deformation analysis. *J. Compos. Mater.* **44**, 5–26. (doi:10.1177/0021998309345348)
11. Charmetant A, Orliac JG, Vidal-Sallé E, Boisse P. 2012 Hyperelastic model for large deformation analyses of 3D interlock composite preforms. *Compos. Sci. Technol.* **72**, 1352–1360. (doi:10.1016/j.compscitech.2012.05.006)
12. Fetfatsidis KA, Jauffrès D, Sherwood JA, Chen J. 2013 Characterization of the tool/fabric and fabric/fabric friction for woven-fabric composites during the thermostamping process. *Int. J. Mater. Forming* **6**, 209–221. (doi:10.1007/s12289-011-1072-5)
13. Allaoui S, Hivet G, Wendling A, Ouagne P, Soulat D. 2012 Influence of the dry woven fabrics meso-structure on fabric/fabric contact behaviour. *J. Compos. Mater.* **46**, 627–639. (doi:10.1177/0021998311424627)
14. Cornelissen B, Sachs U, Rietman B, Akkerman R. 2014 Dry friction characterisation of carbon fibre tow and satin weave fabric for composite applications. *Composites A* **56**, 127–135. (doi:10.1016/j.compositesa.2013.10.006)

15. De Luca P, Pickett AK. 1998 Numerical and experimental investigation of some press forming parameters of two fibre reinforced thermoplastics: APC2-AS4 and PEI-CETEX. *Composites A* **29**, 101–110. (doi:10.1016/S1359-835X(97)00060-2)
16. Hsiao SW, Kikuchi N. 1999 Numerical analysis and optimal design of composite thermoforming process. *Comput. Methods Appl. Mech. Eng.* **177**, 1–34. (doi:10.1016/S0045-7825(98)00273-4)
17. Pickett AK. 2002 Review of finite element methods applied to manufacturing and failure prediction in composite structures. *Appl. Compos. Mater.* **9**, 43–58. (doi:10.1023/A:1012667427575)
18. Boisse P. 2007 Finite element analysis of composite forming. In *Composite forming technologies* (ed. AC Long). Cambridge, UK: Woodhead.
19. Belytschko T. 1983 An overview of semi-discretisation and time integration procedures. In *Computation methods for transient analysis* (eds T Belytschko, TJR Hughes), pp. 1–65. Amsterdam, The Netherlands: Elsevier Science.
20. Hughes TJR, Belytschko T. 1983 A precise of developments in computational methods for transient analysis. *J. Appl. Mech.* **50**, 1033–1041. (doi:10.1115/1.3167186)
21. Crisfield MA. 1997 *Non-linear finite element analysis of solids and structures*, vol. 2. New York, NY: John Wiley & Sons.
22. Zienkiewicz OC, Taylor RL. 2005 *The finite element method for solid and structural mechanics*. London, UK: Butterworth-Heinemann.
23. Belytschko T, Liu WK, Moran B. 2000 *Nonlinear finite elements for continua and structures*. New York, NY: John Wiley & Sons.
24. Onate E, Zarate F. 2000 Rotation-free triangular plate and shell elements. *Int. J. Numer. Methods Eng.* **47**, 557–603. (doi:10.1002/(SICI)1097-0207(20000110/30)47:1/3<557::AID-NME784>3.0.CO;2-9)
25. Hamila N, Boisse P. 2007 A meso–macro three node finite element for draping of textile composite preforms. *Appl. Compos. Mater.* **14**, 235–250. (doi:10.1007/s10443-007-9043-1)
26. Hamila N, Boisse P, Sabourin F, Brunet M. 2009 A semi-discrete shell finite element for textile composite reinforcement forming simulation. *Int. J. Numer. Methods Eng.* **79**, 1443–1466. (doi:10.1002/nme.2625)
27. Hill R. 1958 A general theory of uniqueness and stability in elastic–plastic solids. *J. Mech. Phys. Solids* **8**, 236–249. (doi:10.1016/0022-5096(58)90029-2)
28. Friedl N, Rammerstorfer FG, Fischer FD. 2000 Buckling of stretched strips. *Comput. Struct.* **78**, 185–190. (doi:10.1016/S0045-7949(00)00072-9)
29. Prodromou AG, Chen J. 1997 On the relationship between shear angle and wrinkling of textile composite preforms. *Composites A* **28A**, 491–503. (doi:10.1016/S1359-835X(96)00150-9)
30. Lebrun G, Bureau MN, Denault J. 2003 Evaluation of bias-extension and picture frame test for the measurement of shear properties of PP/glass commingled fabrics. *Compos. Struct.* **61**, 52–341. (doi:10.1016/S0263-8223(03)00057-6)
31. Sharma SB, Sutcliffe MPF, Chang SH. 2003 Characterisation of material properties for draping of dry woven composite material. *Composites A* **34**, 1167–1175. (doi:10.1016/j.compositesa.2003.09.001)
32. Zhu B, Yu TX, Teng J, Tao XM. 2009 Theoretical modeling of large shear deformation and wrinkling of plain woven composite. *J. Compos. Mater.* **43**, 125–138. (doi:10.1177/0021998308098237)
33. Lightfoot JS, Wisnom MR, Potter K. 2013 A new mechanism for the formation of ply wrinkles due to shear between plies. *Composites A* **49**, 139–147. (doi:10.1016/j.compositesa.2013.03.002)
34. Lightfoot JS, Wisnom MR, Potter K. 2013 Defects in woven preforms: formation mechanisms and the effects of laminate design and layup protocol. *Composites A* **51**, 99–107. (doi:10.1016/j.compositesa.2013.04.004)
35. Lee J, Hong S, Yu W, Kang T. 2007 The effect of blank holder force on the stamp forming behaviour of non-crimp fabric with a chain stitch. *Compos. Sci. Technol.* **67**, 357–366. (doi:10.1016/j.compscitech.2006.09.009)
36. Boisse P, Hamila N, Vidal-Sallé E, Dumont F. 2011 Simulation of wrinkling during textile composite reinforcement forming. Influence of tensile, in-plane shear and bending stiffnesses. *Compos. Sci. Technol.* **71**, 683–692. (doi:10.1016/j.compscitech.2011.01.011)

37. Dangora LM, Mitchell CJ, Sherwood JA. 2015 Predictive model for the detection of out-of-plane defects formed during textile-composite manufacture. *Composites A* **78**, 102–112. (doi:10.1016/j.compositesa.2015.07.011)
38. Sjölander J, Hallander P, Åkermo M. 2016 Forming induced wrinkling of composite laminates: a numerical study on wrinkling mechanisms. *Composites A* **81**, 41–51. (doi:10.1016/j.compositesa.2015.10.012)
39. ITOOL 'Integrated Tool for Simulation of Textile Composites'. European Specific Targeted, Research Project, Sixth Framework Programme, Aeronautics and Space. See http://www.itool.eu.
40. Allaoui S, Boisse P, Chatel S, Hamila N, Hivet G, Soulat D, Vidal-Sallé E. 2011 Experimental and numerical analyses of textile reinforcement forming of a tetrahedral shape. *Composites A* **42**, 612–622. (doi:10.1016/j.compositesa.2011.02.001)
41. Allaoui S, Hivet G, Soulat D, Wendling A, Ouagne P, Chatel S. 2014 Experimental preforming of highly double curved shapes with a case corner using an interlock reinforcement. *Int. J. Mater. Forming* **7**, 155–165. (doi:10.1007/s12289-012-1116-5)
42. Tephany C, Gillibert J, Ouagne P, Hivet G, Allaoui S, Soulat D. 2016 Development of an experimental bench to reproduce the tow buckling defect appearing during the complex shape forming of structural flax based woven composite reinforcements. *Composites A* **81**, 22–33. (doi:10.1016/j.compositesa.2015.10.011)
43. Ferretti M, Madeo A, Dell'Isola F, Boisse P. 2014 Modeling the onset of shear boundary layers in fibrous composite reinforcements by second-gradient theory. *Z. Angew. Math. Phys.* **65**, 587–612. (doi:10.1007/s00033-013-0347-8)
44. d'Agostino MV, Giorgio I, Greco L, Madeo A, Boisse P. 2015 Continuum and discrete models for structures including (quasi-)inextensible elasticae with a view to the design and modeling of composite reinforcements. *Int. J. Solids Struct.* **59**, 1–17. (doi:10.1016/j.ijsolstr.2014.12.014)
45. Madeo A, Ferretti M, Dell'Isola F, Boisse P. 2015 Thick fibrous composite reinforcements behave as special second-gradient materials: three-point bending of 3D interlocks. *Z. Angew. Math. Phys.* **66**, 2041–2060. (doi:10.1007/s00033-015-0496-z)
46. ten Thije RHW, Akkerman R. 2008 Solutions to intra-ply shear locking in finite element analyses of fibre reinforced materials. *Composites A* **39**, 1167–1176. (doi:10.1016/j.compositesa.2008.03.014)
47. Hamila N, Boisse P. 2013 Locking in simulation of composite reinforcement deformations. Analysis and treatment. *Composites A* **53**, 109–117. (doi:10.1016/j.compositesa.2013.06.001)
48. Tang XD, Whitcomb JD. 2003 General techniques for exploiting periodicity and symmetries in micromechanics analysis of textile composites. *J. Compos. Mater.* **37**, 1167–1189. (doi:10.1177/0021998303037013003)
49. Lomov SV *et al.* 2007 Meso-FE modelling of textile composites: road map and data flow and algorithms. *Compos. Sci. Technol.* **67**, 1870–1891. (doi:10.1016/j.compscitech.2006.10.017)
50. Lemanski SL, Wang J, Sutcliffe MPF, Potter KD, Wisnom MR. 2013 Modelling failure of composite specimens with defects under compression loading. *Composites A* **48**, 26–36. (doi:10.1016/j.compositesa.2012.12.007)
51. Obert E, Daghia F, Ladeveze P, Ballere L. 2014 Micro and meso modeling of woven composites: transverse cracking kinetics and homogenization. *Compos. Struct.* **117**, 212–221. (doi:10.1016/j.compstruct.2014.06.035)
52. Sekine H, Beaumont PW. 1998 A physically based micromechanical theory of macroscopic stress-corrosion cracking in aligned continuous glass-fibre-reinforced polymer laminates. *Compos. Sci. Technol.* **58**, 1659–1665. (doi:10.1016/S0266-3538(97)00236-4)
53. Xu J, Lomov SV, Verpoest I, Daggumati S, Van Paepegem W, Degrieck J. 2016 A comparative study of twill weave reinforced composites under tension–tension fatigue loading: experiments and meso-modelling. *Compos. Struct.* **135**, 306–315. (doi:10.1016/j.compstruct.2015.09.005)
54. Bickerton S, Simacek P, Guglielmi SE, Advani SG. 1997 Investigation of draping and its effects on the mold filling process during manufacturing of a compound curved composite part. *Composites A* **28**, 801–816. (doi:10.1016/S1359-835X(97)00033-X)
55. Potluri P, Ciurezu DP, Ramgulam RB. 2006 Measurement of meso-scale shear deformations for modelling textile composites. *Composites A* **37**, 303–314. (doi:10.1016/j.compositesa.2005.03.032)

56. Naouar N, Vidal-Sallé E, Schneider J, Maire E, Boisse P. 2014 Meso-scale FE analyses of textile composite reinforcement deformation based on X-ray computed tomography. *Compos. Struct.* **116**, 165–176. (doi:10.1016/j.compstruct.2014.04.026)
57. Naouar N, Vidal-Sallé E, Schneider J, Maire E, Boisse P. 2015 3D composite reinforcement meso FE analyses based on X-ray computed tomography. *Compos. Struct.* **132**, 1094–1104. (doi:10.1016/j.compstruct.2015.07.005)
58. Thompson A, El Said B, Such M, Belnoue JP-H, Hallett SR. Discrete modelling of non-crimp fabric multi-layer preforming processes. In *Proc. 12th Int. Conf. on Textile Composites (TEXCOMP-12), 26–29 May 2015, Raleigh, NC, USA*.
59. Isart N, El Said B, Ivanov DS, Hallett SR, Mayugo JA, Blanco N. 2015 Internal geometric modelling of 3D woven composites: a comparison between different approaches. *Compos. Struct.* **132**, 1219–1230. (doi:10.1016/j.compstruct.2015.07.007)
60. Bayraktar H, Ehrlich D, Scarat G, McClain M, Timoshchuk N, Redman C. 2015 Forming and performance analysis of a 3D-woven composite curved beam using meso-scale FEA. *SAMPE Journal* **51**, 23–29.
61. Badel P, Vidal-Sallé E, Boisse P. 2008 Large deformation analysis of fibrous materials using rate constitutive equations. *Comput. Struct.* **86**, 1164–1175. (doi:10.1016/j.compstruc.2008.01.009)
62. Bareggi A. 2012 Mesoscopic analyses of textile composite reinforcement forming. Internal Report, LaMCoS, INSA Lyon.
63. Gatouillat S, Bareggi A, Vidal-Sallé E, Boisse P. 2013 Meso modelling for composite preform shaping–simulation of the loss of cohesion of the woven fibre network. *Composites A* **54**, 135–144. (doi:10.1016/j.compositesa.2013.07.010)